Laine, Sampo; Hakonen, Urho; Hartikainen, Hannu; Viitala, Raine

Frequency domain solution method for electromagnetic influence analysis on torsional vibrations

Published in:
Journal of Sound and Vibration

DOI:
10.1016/j.jsv.2024.118780

Published: 05/02/2025

Journal of Sound and Vibration 596 (2025) 118780

Contents lists available at ScienceDirect

Journal of Sound and Vibration

journal homepage: www.elsevier.com/locate/jsvi

Frequency domain solution method for electromagnetic influence analysis on torsional vibrations[☆]

Sampo Laine[a,*], Urho Hakonen[a], Hannu Hartikainen[b], Raine Viitala[a]

[a] Department of Mechanical Engineering, Aalto University, P.O. Box 14300, 00076 Aalto, Finland
[b] Department of Electrical Engineering, Aalto University, P.O. Box 14300, 00076 Aalto, Finland

ARTICLE INFO

Keywords:
Structural dynamics
Torsional vibration
Electric machine
Induction motor
Electromechanical interaction

ABSTRACT

In electric motor-driven machines, mechanical torsional dynamics are nonlinearly coupled with the electrical system through the electromagnetic torque and the counter-electromotive force. In this paper, an approach based on small-signal linearization is proposed for modeling the steady-state torsional dynamics of the coupled system. Using the linearized model, resonance interference diagrams, torsional response, and stability can be evaluated rapidly across numerous operating points, while accurately accounting for the electromagnetic effects. The model is validated with conventional time-stepping simulations of two induction machines. An example analysis of a 3 MW motor-driven compressor train displays the modification of torsional properties due to the electromagnetic coupling effect and explains the mechanism of torsional destabilization. Finally, previously published measurements of a 37 kW motor test bench are considered to validate the instability of the elastic torsional mode predicted by the model.

1. Introduction

Torsional vibration analysis is a standard procedure in the design of large rotating machinery. The importance of accurate analysis is highlighted in reciprocating machinery, where large torque oscillations are present. In the conventional methods for torsional vibration analysis, a mechanical model of the system is established, and its response is studied to various sources of torque excitations. This method requires that the excitation frequencies and their amplitudes are known. It is well known, that torque ripple is caused in voltage source inverter drives. These excitations originate from the discrete switching of the input voltage, as well as from the modulated DC-link voltage ripple [1–3]. It is possible to adjust the frequency of these excitations with the modulating frequency ratio to avoid exciting torsional resonances [4]. In many electric machine types, the cogging torque is a significant source of torque pulsations. In permanent magnet motors, the identified torque ripple caused by the cogging torque originating from the interaction of the rotor permanent magnets and the stator slots can be applied as a mechanical excitation to study the response of the system [5]. When induction motors are considered, ignoring the dynamics of the electrical subsystem and treating the torque as an external input can lead to inaccurate modeling results. For this reason, a model combination approach is required to accurately describe the coupled dynamics of the mechanical and electrical subsystems.

Since a long time ago, it has been known that the torsional mechanical and electrical systems are connected through the mechanical rotational angle and the electromagnetic torque produced by the motor [6]. In principle, energy transfer occurs between electromagnetic potential energy and the torsional spring of the flexible mechanical system. Increase in natural frequencies of the

☆ Funding: This work was supported by the Academy of Finland, Finland grant number 346443, and Business Finland grant number 243/31/2022.

* Corresponding author.
E-mail address: sampo.laine@aalto.fi (S. Laine).

https://doi.org/10.1016/j.jsv.2024.118780
Received 23 May 2024; Received in revised form 29 August 2024; Accepted 26 September 2024
Available online 24 October 2024
0022-460X/

mechanical system is observed due to the electromagnetic stiffness. Self-excited torsional vibrations may arise in the case of negative electromagnetic damping. Tabesh and Iravani [7] proposed a frequency response approach derived from a small-signal model of an electric machine for analysis of torsional vibrations. In this approach, the frequency response from rotor angle to electromagnetic torque is directly interconnected with the mechanical system. This model, consisting of electrical and mechanical frequency responses, works for both synchronous and asynchronous motors. The frequency response approach has been further considered for identifying computationally efficient equivalent circuit parameters from electromagnetic finite element models [8–10]. Identifying the motor equivalent circuit parameters enables studying the dynamics even before the motor is manufactured, making these models especially suitable for design phase torsional vibration analyses. In practical analyses, the frequency dependent dynamics are sometimes omitted, and constant equivalent stiffness and damping values are used in torsional analyses to account for the electromagnetic stiffening effect [11]. Using constant equivalent stiffness and damping parameters assumes, that the electromagnetic effect is not operating point dependent.

Time-stepping simulation is typically used for analysis of torsional vibrations in electric drive systems. The electromagnetic components show a nonlinear response, which complicates the use of analytic solutions, thus the majority of authors have relied on time-stepping simulations. Several application papers have established models for simulating the interconnected electrical and mechanical systems for analysis of torsional vibrations. Thorsen and Dalva used time-stepping simulation to model the coupled torsional dynamics of an induction motor driven submersible pump [12]. Zhang et al. used a coupled model to study a wind turbine drivetrain and the permanent magnet synchronous generator. This system had additional nonlinearities due to the time-varying meshing stiffness of the gears [13]. Shi et al. established an electromechanical model to analyze torsional vibrations in a planetary gear transmission driven by an asynchronous motor [14]. Wang et al. established an electromechanical model of an inverter supplied differential speed regulation system. The model was then used to study the dynamics with time-domain simulation in several operating conditions [15]. A similar approach was adopted in [16] to study the electromechanical coupling characteristics in a dual motor electric maritime propulsion system. In [17], a combined electrical and mechanical simulation model was used to detect parameters related to gear tooth deformations. Zhou et al. [18] simulated the dynamic coupling effects in railway application subject to excitations originating from gear meshing and wheel–rail interactions.

Lumped-element mechanical models have been applied in the development of control systems with the aim of reducing torsional vibrations [19–22]. Unlike the instabilities in lateral rotordynamics due to the cross coupling terms in the stiffness matrix, such as the oil whip, torsional instabilities are rarely encountered in the field. In electric drives, torsional instability can originate from the interconnection of the mechanical and electrical subsystems [23]. Some of the instabilities can be modeled using a torsionally rigid mechanical model. The unstable torsional modes are manifested as speed and torque oscillations [24–26]. All of these torsional instabilities arising from the electromechanical interaction are also highly dependent on the applied control system [27], thus, omitting the control in the analysis may lead to significant inaccuracies.

There have been many research works devoted to applying the equivalent circuit models in simulation of torsional vibrations [28–30]. Time-stepping simulation of the entire non-linear dynamics has been demonstrated effective, but is often not used in practical torsional analyses due to the computational burden and software limitations. In [31], the electromagnetic damping and stiffness identified from the frequency response were used to simulate the electromagnetic coupling effect in geared systems. Tan et al. used the electromagnetic stiffness in modal analysis of a windmill [32]. As discussed in [33], the identified electromagnetic stiffness and damping offer a simple way to linearize the electromagnetic interaction. However, using single values for the electromagnetic stiffness and damping leads to major simplification of the dynamics. In [34], the harmonic balance method was applied to compute an analytic solution for the electromechanical interconnection. This approach is effective in linearizing the electrical subsystem in steady-state conditions, but requires numerical iteration for the solution coefficients. In general, the interconnection of the mechanical and electrical subsystems is nonlinear and operating point dependent. For this reason, most of the previous works have relied on time-stepping simulations in solving the coupled system of equations.

The aim of this research is to improve on the current state-of-the-art solution methods by deriving a frequency domain solution, which accurately incorporates the electromagnetic influence. The main contributions of this article can be summarized as follows

1. Coupled system model of an induction motor and drivetrain including the control model is derived and linearized in a steady-state operating point. The operating point is defined with three free parameters as described in Section 2. The proposed formulation allows for rapid calculations across several operating points.
2. In Section 4, a harmonic steady-state solution to the coupled forced vibration problem is derived in the second order form commonly used in structural dynamics. The response calculations are verified with conventional non-linear simulations of the coupled model. A variable speed compressor train, displaying significant electromagnetic coupling effects is presented as an application example.
3. Self excited torsional vibrations originating from the feedback mechanism of the electromagnetic coupling are further examined and compared with measurements. The analysis shows that unstable torsional vibrations can originate due to the coupling of the electrical subsystem and the elastic torsional mode.

2. Electrical model

The widely used T-equivalent circuit model is used to model the induction motor [35]. The three-phase voltage is transformed to the dq-frame. The real vector form is used for the space-vector quantities, denoted as $\boldsymbol{i} = \begin{bmatrix} i_\mathrm{d} & i_\mathrm{q} \end{bmatrix}^\mathrm{T}$ for the currents and $\boldsymbol{u} = \begin{bmatrix} u_\mathrm{d} & u_\mathrm{q} \end{bmatrix}^\mathrm{T}$ for the voltages. In the following equations, the orthogonal rotation matrix is defined as $\mathbf{J} = \begin{bmatrix} \begin{bmatrix} 0 & -1 \end{bmatrix}, \begin{bmatrix} 1 & 0 \end{bmatrix} \end{bmatrix}$. The circuit model

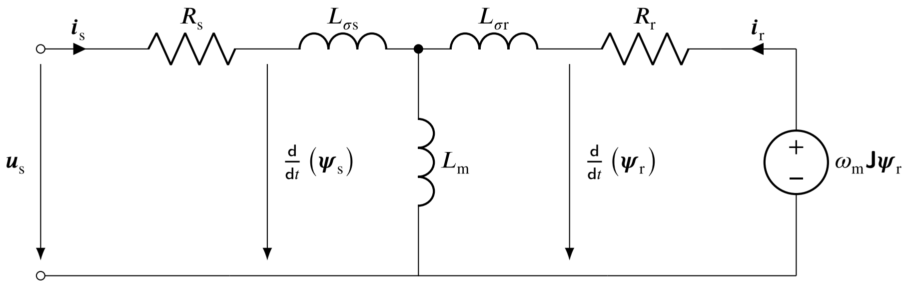

Fig. 1. T-equivalent circuit of an induction motor.

is displayed in Fig. 1. In the synchronous coordinates, i.e., in a reference coordinate frame rotating with the angular speed of a reference frame ω_s, the voltage equations are

$$\begin{aligned} \boldsymbol{u}_{\mathrm{s}} &= R_{\mathrm{s}}\boldsymbol{i}_{\mathrm{s}} + \frac{\mathrm{d}\boldsymbol{\psi}_{\mathrm{s}}}{\mathrm{d}t} + \mathbf{J}\omega_{\mathrm{s}}\boldsymbol{\psi}_{\mathrm{s}} \\ \mathbf{0} &= R_{\mathrm{r}}\boldsymbol{i}_{\mathrm{r}} + \frac{\mathrm{d}\boldsymbol{\psi}_{\mathrm{r}}}{\mathrm{d}t} + \mathbf{J}(\omega_{\mathrm{s}} - \omega_{\mathrm{m}})\boldsymbol{\psi}_{\mathrm{r}} \end{aligned} \tag{1}$$

where R_{s} is the stator resistance, R_{r} is the rotor resistance, $\boldsymbol{\psi}_{\mathrm{s}}$ is the stator flux linkage, $\boldsymbol{\psi}_{\mathrm{r}}$ is the rotor flux linkage, ω_{m} is the electrical angular frequency of the motor. The subtraction $\omega_{\mathrm{s}} - \omega_{\mathrm{m}}$ is the slip of the motor ω_{r}. The non-linearity of the model originates from the induced voltage of rotation, which is described by the last terms on the right hand side of the equations. In this nonlinear dynamic model, the flux linkages can be further expressed in terms of currents by the relations

$$\begin{aligned} \boldsymbol{\psi}_{\mathrm{s}} &= L_{\mathrm{s}}\boldsymbol{i}_{\mathrm{s}} + L_{m}\boldsymbol{i}_{\mathrm{r}} \\ \boldsymbol{\psi}_{\mathrm{r}} &= L_{\mathrm{m}}\boldsymbol{i}_{\mathrm{s}} + L_{\mathrm{r}}\boldsymbol{i}_{\mathrm{r}} \end{aligned} \tag{2}$$

where L_{m} is the magnetizing inductance. Identities ($L_{\mathrm{s}} = L_{\sigma s} + L_{\mathrm{m}}$) and ($L_{\mathrm{r}} = L_{\sigma\mathrm{r}} + L_{\mathrm{m}}$) are applied, where the inductances $L_{\sigma s}$ and $L_{\sigma\mathrm{r}}$ correspond to the equivalent circuit in Fig. 1. Stacking the stator and rotor currents in one vector $\boldsymbol{i}$ and selecting it as the vector of free variables, this nonlinear large-signal model of an induction motor can be alternatively described in the matrix form

$$\boldsymbol{u} = \mathbf{L}\frac{\mathrm{d}}{\mathrm{d}t}(\boldsymbol{i}) + \mathbf{R}\boldsymbol{i}, \tag{3}$$

where $\mathbf{L}$ is the inductance matrix, and $\mathbf{R}$ is the resistance matrix. The vector $\boldsymbol{u}$ contains the stator and rotor currents. From this equation, the state-space representation is obtained as follows

$$\frac{\mathrm{d}}{\mathrm{d}t}(\boldsymbol{i}) = -\mathbf{L}^{-1}\mathbf{R}\boldsymbol{i} + \mathbf{L}^{-1}\mathbf{u}. \tag{4}$$

Non-linearity of the model follows from the product of the rotating speed ω_{m} and the rotor flux linkage $\boldsymbol{\psi}_{\mathrm{r}}$ in the rotor voltage equation (Eq. (1)), which cannot be separated in the state-space form.

Simulating this model is straight-forward and only requires a model for the voltage supply. The model can be connected to mechanical equations of motion through the mechanical variables, which are the electromagnetic torque τ_{m} acting on the rotor, and the electrical angular speed of the rotor ω_{m}. The electromagnetic torque can be written as

$$\tau_{\mathrm{m}} = \frac{3p}{2}\boldsymbol{i}_{\mathrm{s}}^{\mathrm{T}}\mathbf{J}\boldsymbol{\psi}_{\mathrm{s}} \tag{5}$$

where p is the number of pole pairs.

Identification of the model parameters is one of the most important considerations for the accuracy of these equivalent circuit models. The motor models can be identified through experimental or numerical methods [8–10]. Parameter identification is a standard procedure in deployment of drive systems, while numerical methods employing electromagnetic finite element methods may be used in the design of motors. It has been shown, that even the most simple equivalent circuit models can reach reasonable accuracy in comparison with the two-dimensional FE models with properly conducted parameter identification [8]. The T-equivalent circuit model could also be extended to include flux saturation characteristics and skin effect of rotor bars [36].

Two induction motors are used in the calculations. Parameters of the motors are given in Table 1. The first motor is a 37 kW induction machine discussed in [10]. The equivalent circuit parameters of this model are identified from time-harmonic finite element analysis fitting procedure. This motor model has also been compared to experiments in a previous study [37]. The second motor is a 3.7 MW induction machine, described in [9]. Similarly to the electrical parameters of this motor have also been estimated from finite element analysis and validated against the electromagnetic finite element model.

2.1. Control system

To study the electromagnetic effects in variable speed operation, standard V/Hz control is considered. A block-diagram of the control system is given in Fig. 2. Two feed-forward gains from the stator current estimate are used, namely, RI-compensation and

Table 1
Parameters of the two induction motors.

Parameter	Symbol	Value		Unit
		Motor 1	Motor 2	
Power	P	37	3725	kW
Frequency	f	50	60	Hz
Pole pairs	p	2	4	–
Rated voltage	U	$\frac{\sqrt{2}}{\sqrt{3}}400$	$\frac{\sqrt{2}}{\sqrt{3}}4000$	V
Rated torque	τ_{rated}	248	37 000	N m
Rotor Inertia	I_{m}	0.26	219.9	kg m^2
Stator resistance	R_{s}	83.6	23.5	mΩ
Rotor resistance	R_{r}	66.8	19.5	mΩ
Stator self-inductance	L_{s}	27.6	30.5	mH
Rotor self-inductance	L_{r}	28.4	30.0	mH
Magnetizing inductance	L_{m}	26.8	28.9	mH

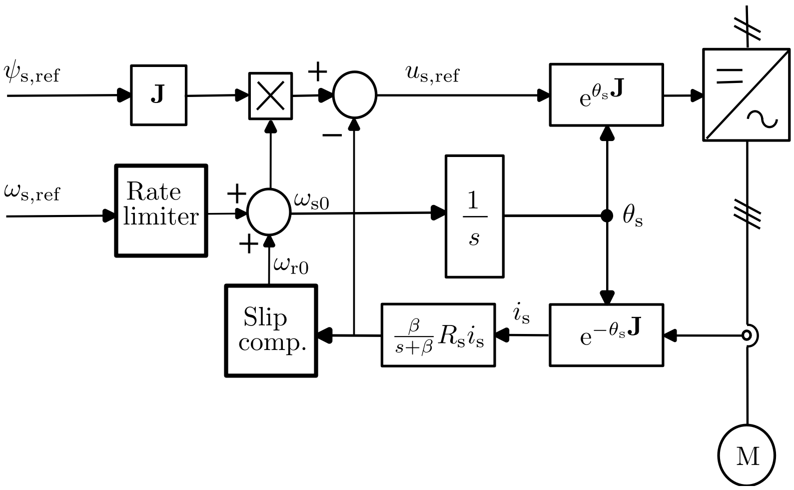

Fig. 2. Block diagram of the V/Hz control used in the simulations.

slip compensation. RI-compensation is essential for the stability of the control system in low rotating speeds, and slip compensation is applied for more accurate speed control. The PWM voltage reference is defined as

$$\boldsymbol{u}_{\mathrm{s,ref}} = R_{\mathrm{s}}\boldsymbol{i}_{\mathrm{s0}} + \omega_s \mathbf{J}\boldsymbol{\psi}_{\mathrm{s0}}, \tag{6}$$

where the first term is the RI-compensation, and the second term is the slip compensation. Subscript 0 refers to the quasi-constant operating point quantities. In simulations, the steady-state stator current is calculated from the low-pass filtered stator current. In the linearization, the dynamics of this low-pass filter are omitted as its influence on the relatively low frequency mechanical vibrations is minor.

$$\frac{1}{\beta}\frac{\mathrm{d}\boldsymbol{i}_{\mathrm{s0}}}{\mathrm{d}t} + \boldsymbol{i}_{\mathrm{s0}} = \boldsymbol{i}_{\mathrm{s}}, \tag{7}$$

where β is the bandwidth of the filter. The stator voltage reference ω_s is estimated from the steady-state motor speed and slip frequency

$$\omega_{\mathrm{s}} = \omega_{\mathrm{m0}} + \omega_{\mathrm{r0}}. \tag{8}$$

2.2. Operating point

The nonlinear large-signal motor is studied in steady-state operation, where $\frac{\mathrm{d}}{\mathrm{d}t} = 0$. The operating point of the motor is defined by the stator flux linkage ψ_{s0}, stator frequency u_{s0} and torque τ_{m0}. Ideal RI and slip compensators are assumed. Further assumptions for the rotor voltage would be required in the case of slip ring machines, such as ones presented in [38]. When the steady-state currents are calculated, constant stator flux linkage can be assumed. In the present analyses, stator flux linkage magnitude based on rated values is used $|\boldsymbol{\psi}_{\mathrm{s0}}| = u_{\mathrm{rated}}/\omega_{\mathrm{rated}}$. In the field-weakening region, the stator flux linkage is inversely proportional to the stator frequency ω_{s0}. The steady-state stator currents can be subsequently calculated for any input frequency from this relation. From these

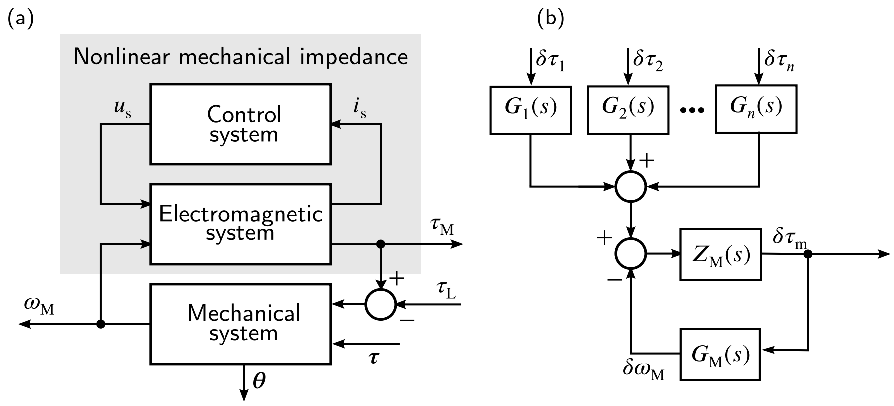

Fig. 3. The nonlinear interconnections between the subsystems are shown in (a), the linearized model is seen in (b) $Z_M(s)$ is the linearized mechanical impedance of the electrical subsystem, and the transfer functions $G_1(s) - G_n(s)$ are the transfer functions of the mechanical subsystem, one for each lumped-mass element. $G_M(s)$ is the transfer function of the lumped element associated with the motor.

quantities, the rest of the operating point parameters can be solved using the steady-state equations. First, the rotor current is solved from Eq. (2)

$$\boldsymbol{i}_{r0} = \frac{1}{L_m}\boldsymbol{\psi}_{s0} - \frac{L_s}{L_m}\boldsymbol{i}_{s0}. \tag{9}$$

Substitution of Eq. (9) to the rotor voltage equation gives

$$\boldsymbol{i}_{s0} = (R_r L_s \mathbf{I} - \omega_{r0} L_m^2 \mathbf{J} + L_s L_r \omega_{r0} \mathbf{J})^{-1}(R_r \mathbf{I} + L_r \omega_{r0} \mathbf{J})\boldsymbol{\psi}_{s0}. \tag{10}$$

Finally, the solved stator current is substituted electromagnetic torque expression (Eq. (5)), which simplifies to

$$\tau_{m0} = \frac{3p}{2} \frac{L_m^2 R_r \omega_{r0} \psi_{s0}^2}{\omega_{r0}^2 \left(L_m^2 - L_r L_s\right)^2 + L_s^2 R_r^2}. \tag{11}$$

This resulting polynomial could be solved for an analytic expression for the slip speed ω_{r0} in terms of the magnitude of the stator flux linkage and motor torque. With the Eqs. (9)–(11), the operating point is uniquely defined by the three scalar variables ψ_{s0}, ω_{s0} and τ_{m0}.

2.3. Linearized small-signal model

The considered linearization approach based on small-signal modeling is shown in Fig. 3. The small signal model is a standard method for analyzing the stability and passivity of an electric machine drive [7,23,27,39]. The small signal model is valid for small perturbations around the operating point. The small signal model could contain different characteristics of the motor or control methods [27,36,40]. In general, the small-signal linearization is valid only in the steady-state conditions. In the analysis, the inverter is assumed to be ideal, i.e., $\boldsymbol{u}_{s,ref} = \boldsymbol{u}_s$, and parameter errors are omitted. The small-signal model is derived by substituting the large-signal variables with small deviations from an operating point, and subtracting the constant steady-state equilibrium from the resulting equations. The small signal variations are denoted as $\delta\omega = \omega - \omega_0$, where the subscript 0 refers to steady-state quantities. Since the mechanical system is already linear, only the electrical subsystem has to be considered.

Expressed in matrix form of Eq. (3), the small-signal linearized voltage and torque equations are

$$\underbrace{\begin{bmatrix} \delta u_{sx} \\ \delta u_{sy} \\ \delta u_{rx} \\ \delta u_{ry} \\ \delta\tau_m \end{bmatrix}}_{\delta \boldsymbol{u}} = \underbrace{\begin{bmatrix} L_s & 0 & L_m & 0 & 0 \\ 0 & L_s & 0 & L_m & 0 \\ L_m & 0 & L_r & 0 & 0 \\ 0 & L_m & 0 & L_r & 0 \\ 0 & 0 & 0 & 0 & 0 \end{bmatrix}}_{\mathbf{L}} \frac{\mathrm{d}}{\mathrm{d}t} \left(\underbrace{\begin{bmatrix} \delta i_{sd} \\ \delta i_{sq} \\ \delta i_{rd} \\ \delta i_{rq} \\ \delta\omega_M \end{bmatrix}}_{\delta \boldsymbol{i}} \right) + \underbrace{\begin{bmatrix} R_s & -\omega_{s0} L_s & 0 & -\omega_{s0} L_m & 0 \\ \omega_{s0} L_s & R_s & \omega_{s0} L_m & 0 & 0 \\ 0 & -\omega_{r0} L_m & R_r & -\omega_{r0} L_r & p(L_r i_{rq0} + L_m i_{sq0}) \\ \omega_{r0} L_m & 0 & \omega_{r0} L_r & R_r & -p(L_m i_{sd0} + L_r i_{rd0}) \\ \frac{3pL_m}{2} i_{rq0} & -\frac{3pL_m}{2} i_{rd0} & -\frac{3pL_m}{2} i_{sq0} & \frac{3pL_m}{2} i_{sd0} & 0 \end{bmatrix}}_{\mathbf{R}} \underbrace{\begin{bmatrix} \delta i_{sd} \\ \delta i_{sq} \\ \delta i_{rd} \\ \delta i_{rq} \\ \delta\omega_M \end{bmatrix}}_{\delta \boldsymbol{i}} \tag{12}$$

where $\omega_M = \omega_m / p$ is the mechanical motor speed. The steady-state currents found in the expression can be calculated directly from the steady-state solutions Eqs. (9) and (10). The steady-state slip angular frequency ω_{r0} can be solved from Eq. (11).

The transfer function from motor angular speed to the electromagnetic torque can be used to explain the influence of the electromagnetic effect on the torsional dynamics.

$$Z_M(s) = \frac{\delta\tau_m(s)}{\delta\omega_M(s)} \tag{13}$$

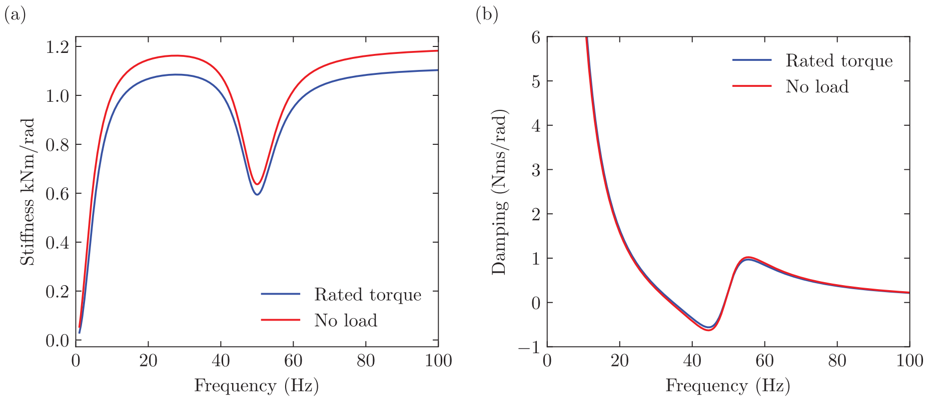

Fig. 4. Electromagnetic (a) Stiffness and (b) damping components of the mechanical impedance at rated speed of the 37-kW motor in the rated torque and no-load conditions. The stiffness and damping coefficients are operating-point dependent, as well as frequency dependent.

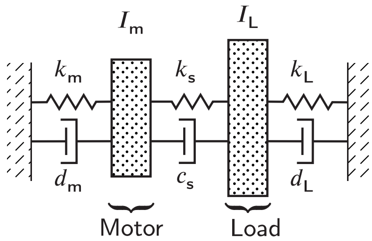

Fig. 5. The two-mass mechanical model is a simple model that can be used to study torsional vibrations in a motor connected to the driven load.

Fluctuations in the rotor speed induces a voltage through the back-electromotive force, which in turn affects the electromagnetic torque produced by the motor. An analytic solution for the transfer function can be derived in a steady-state operating point. Derivation of the transfer function is presented in Appendix A. The frequency response associated with this transfer function, i.e., mechanical impedance, can be used to derive electromagnetic stiffness and damping components of an equivalent mechanical system [41]. A larger electromagnetic influence on the torsional dynamics can be expected if the electromagnetic stiffness and damping are not negligible in comparison to the damping and stiffness of the mechanical system. The mechanical impedance of the electrical subsystem is operating point specific and the derived damping and stiffness parameters vary with the frequency. The mechanical impedance could also be directly identified from simulations [42]. The electromagnetic damping and stiffness coefficients of a 37-kW motor at the rated speed. Rated torque and no-load conditions are shown in Fig. 4.

3. Mechanical model

This section describes the lumped-element mechanical system models that are used in calculating torsional vibration responses. The mechanical model consists of the torsional system and excitation models. The same torsional model can be used in transient and steady-state analysis. These equations of motion presented in this section are later used as a basis of the electromechanical system model. The torsional excitation model described in this chapter is also used later in the electromechanical simulations. Fig. 5 presents a simple two degree-of-freedom lumped-element model. The first torsional mode of any mechanical system can be simplified to this model with lumped parameters. The model consists of two lumped inertias I_m and I_L connected by a torsional spring with stiffness k_s and damping c_s. The inertias are connected to the ground by external torsional springs with stiffnesses k_m, k_L and damping d_m, d_L respectively. The external damping results from the interaction of rotating and non-rotating elements.

3.1. Natural frequencies and mode shapes

The mechanical model of torsional dynamics can be created using continuous and lumped elements discretized along the shaft line. This approach is often referred to as the shaft-line finite element method. Many of the computer programs used in torsional vibration analysis employ this method, where the mechanical model is formed by considering the rotational angles of each node of the discretized system. The matrix form equations of motion for this model can be extended to any number of degrees-of-freedom.

The equations of motion for the second order flexible mechanical system can be written as

$$\mathbf{M}\frac{\mathrm{d}}{\mathrm{d}t^2}(\boldsymbol{\theta}) + \mathbf{C}\frac{\mathrm{d}}{\mathrm{d}t}(\boldsymbol{\theta}) + \mathbf{K}\boldsymbol{\theta} = \boldsymbol{\tau}, \tag{14}$$

where $\mathbf{M}$, $\mathbf{C}$, $\mathbf{K}$ are the mass, damping and stiffness matrices, respectively. These matrices are obtained from the finite element model of the torsional system. $\boldsymbol{\tau}$ is the vector of external torques, and $\boldsymbol{\theta}$ is the vector of the rotational angles for each node.

The torsional natural frequencies and the associated mode shapes can be investigated by transforming the second-order system of Eq. (14) by stacking the state variable vector together with its time-derivative. The system can be rewritten in the state-space form

$$\frac{d}{dt}\left\{\begin{matrix}\boldsymbol{\theta}\\ \frac{\mathrm{d}}{\mathrm{d}t}(\boldsymbol{\theta})\end{matrix}\right\} = \begin{bmatrix}\mathbf{0} & \mathbf{I}\\ -\mathbf{M}^{-1}\mathbf{K} & -\mathbf{M}^{-1}\mathbf{C}\end{bmatrix}\left\{\begin{matrix}\boldsymbol{\theta}\\ \frac{\mathrm{d}}{\mathrm{d}t}(\boldsymbol{\theta})\end{matrix}\right\} + \left\{\begin{matrix}\mathbf{0}\\ \mathbf{M}^{-1}\end{matrix}\right\}\boldsymbol{\tau}. \tag{15}$$

The damped torsional natural frequencies are given by the imaginary parts of the eigenvalues of the system matrix, and the eigenvectors the corresponding mode shapes. Moreover, this model can be used to simulate the system in time-domain.

3.2. Excitation model

Torsional excitations are often harmonics of the fundamental frequency. Many vibration sources of rotating systems originate from the rotating motion of the shaft. These effects include unbalance, misalignment, impellers, fans and gear meshing vibrations. Additionally, there are sources of vibration whose frequencies are not related to the rotating speed, but they are not common in torsional analyses.

When a torsional system is simulated using time-stepping integration, the excitation harmonics have a frequency which depends on the rotating speed. These harmonic torque excitations can be implemented in the simulation for n harmonics as

$$\tau(t) = \sum_n X_n \cos\left(f_n \int_{t_0}^{t_1} \omega_{\mathrm{M}}(t)\mathrm{d}t + \phi_n\right), \tag{16}$$

where $\tau(t)$ is the excitation torque, f_n is the multiplier of the fundamental frequency, ω_{M} is the rotating speed, X_n is the amplitude, and ϕ_n is the initial phase of the n:th frequency component. It is important to use the integral of the speed instead of the frequency to maintain correct phase of the excitation. This general excitation model can be used to approximate any periodic excitation which has frequency proportional to the rotating frequency.

3.3. Harmonic solution and vibratory torque

In torsional vibration analysis, the torsional stresses acting on a drivetrain are typically inspected by calculating forced responses, from which the vibratory torque is calculated. Vibratory torque is the oscillating component of the torque through a torque transferring system. Calculating the torsional responses using the harmonic models has been widely adopted, as the harmonic response has an analytic solution. The analytic solution is calculated rapidly in comparison to time-stepping simulation. Fast solution time is especially useful in torsional analysis, where the responses are often calculated for large number of operating conditions and excitation cases.

According to the superposition principle, the steady-state forced response of a linear system can be calculated as a sum of its frequency components. The assumed model for the rotating angles of each degree-of-freedom is

$$\theta(t) = \mathrm{Re}\left(\sum_k a_k e^{j(\omega_k t + \phi_k)}\right) \tag{17}$$

where a is the magnitude, and ω_k and ϕ_k are the angular frequency and phase of the vibrations, respectively. It should be noted, that the frequency components of the response are most likely related to the operating speed. The response to the harmonic excitation in terms of rotating angles can be calculated using the receptance matrix

$$\boldsymbol{\theta}_n = \left(-\mathbf{M}\omega_n^2 + \mathbf{C}j\omega_n + \mathbf{K}\right)^{-1}\boldsymbol{\tau}_n, \tag{18}$$

where $\boldsymbol{\tau}_n$ and $\boldsymbol{\theta}_n$ are complex valued vectors of the input torques and vibration outputs of the system at n:th frequency component. Furthermore, the vibratory torque for each α:th element at n:th frequency is

$$T_{\alpha,n} = k_\alpha(\theta_{\alpha,n+1} - \theta_{\alpha,n}) + c_\alpha(j\omega_n\theta_{\alpha,n+1} - j\omega_n\theta_{\alpha,n}), \tag{19}$$

where k_α and c_α are the torsional stiffness and damping of the α:th element.

The vibratory torque amplitude of each element is the absolute value of the vibratory torque. The vector of total vibratory torque $\boldsymbol{T}$ at each rotating speed can thus be calculated as the sum of the vectors corresponding to all frequency components

$$\boldsymbol{T} = \sum_n |\boldsymbol{T}_n|. \tag{20}$$

The steady-state response can be simulated by numerically integrating the state derivatives of Eq. (15). The simulation result is post-processed through Eq. (20), which gives the instantaneous shaft torque at each time-step. Finally, the simulated vibratory torque is estimated as the amplitude of the shaft torque signal. In presence of multiple excitation frequencies, the maximum peak-to-peak value in the steady-state signal is used. Fig. 6 illustrates the steady-state vibrations of the two-mass mechanical model. The system response is simulated with the excitation model given in Eq. (16).

The vibratory torque response can be calculated directly using the harmonic solution of Eq. (18). The harmonic solution for the entire speed range can be calculated in a fraction of a second, while a separate time-stepping simulation is required for each simulated response. In this case, where the non-linear effects are negligible, the amplitude of the simulated responses are close to equal to the ones of the harmonic solution.

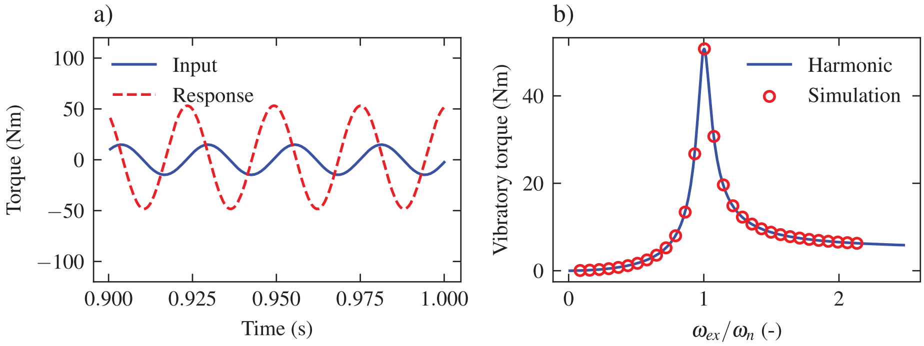

Fig. 6. The mechanical system response is simulated at each rotating speed. A steady-state portion of a single simulation where rotating speed is 215 rad/s is shown in (a). In (b), the harmonic solution is plotted together with multiple simulated response amplitudes. Similar comparisons of the simulated and calculated analytic responses are considered later in the electromechanical cases.

4. Coupled system model

In conventional torsional vibration analysis, the input excitations are typically considered as ideal external torques, omitting the feedback dynamics of the electric motor. The frequency response approach considered in previous works allows including the motor dynamics, but a different frequency response has to be known for all considered operating points [42]. In the approach proposed in this paper, the linearized motor model is connected directly with the mechanical model. This approach allows computing analytic solutions without the pre-computation of frequency responses.

The previously described mechanical and electrical models can be combined to yield a combined linear system model in an operating point. When the electrical model is presented in the second order form, aggregation of the electrical and mechanical system matrices is straight-forward. The second order form of the coupled differential equations can be written in the block matrix notation as

$$\underbrace{\begin{bmatrix} \mathbf{L}_{11} & \mathbf{l}_{12} & 0 \\ \mathbf{l}_{21} & l_{22}+m_{11} & \mathbf{m}_{12} \\ 0 & \mathbf{m}_{21} & M_{22} \end{bmatrix}}_{\mathbf{M}_c} \delta\ddot{\boldsymbol{x}} + \underbrace{\begin{bmatrix} \mathbf{R}_{11} & \mathbf{r}_{12} & 0 \\ \mathbf{r}_{21} & r_{22}+c_{11} & \mathbf{c}_{12} \\ 0 & \mathbf{c}_{21} & C_{22} \end{bmatrix}}_{\mathbf{C}_c} \delta\dot{\boldsymbol{x}} + \underbrace{\begin{bmatrix} \mathbf{0}_{11} & \mathbf{0}_{12} & 0 \\ \mathbf{0}_{21} & 0_{22}+k_{11} & \mathbf{k}_{12} \\ 0 & \mathbf{k}_{21} & K_{22} \end{bmatrix}}_{\mathbf{K}_c} \delta\boldsymbol{x} = \delta\boldsymbol{z}, \tag{21}$$

where the matrices $\mathbf{L}$ and $\mathbf{R}$ are the electrical matrices from Eq. (3) and the matrices $\mathbf{M}$, $\mathbf{C}$, $\mathbf{K}$ are the mechanical matrices from Eq. (14). The state derivatives of the coupled model can be calculated as

$$\frac{\mathrm{d}}{\mathrm{d}t}\left(\begin{Bmatrix} \delta\boldsymbol{x} \\ \frac{\mathrm{d}}{\mathrm{d}t}(\delta\boldsymbol{x}) \end{Bmatrix}\right) = \underbrace{\begin{bmatrix} \mathbf{0} & \mathbf{I} \\ -\mathbf{M}_c^{-1}\mathbf{K}_c & -\mathbf{M}_c^{-1}\mathbf{C}_c \end{bmatrix}}_{\mathbf{A}_c} \begin{Bmatrix} \delta\boldsymbol{x} \\ \frac{\mathrm{d}}{\mathrm{d}t}(\delta\boldsymbol{x}) \end{Bmatrix} + \begin{Bmatrix} \mathbf{0} \\ \mathbf{M}_c^{-1} \end{Bmatrix} \delta\boldsymbol{z} \tag{22}$$

The state-vector of this system is consists of the mechanical rotation angles and the integrals of the stator and rotor currents

$$\begin{aligned} \delta\boldsymbol{x} &= \begin{bmatrix} \delta q_{sd} & \delta q_{sq} & \delta q_{rd} & \delta q_{rq} & \delta\theta_1 & .. & \delta\theta_n \end{bmatrix}^{\mathrm{T}} \\ \delta\boldsymbol{z} &= \begin{bmatrix} \delta u_{sd} & \delta u_{sq} & \delta u_{rd} & \delta u_{rq} & \delta\tau_1 & .. & \delta\tau_n \end{bmatrix}^{\mathrm{T}} \end{aligned} \tag{23}$$

where q is the electric charge, defined as an integral of the current

$$q = \int_0^t i \mathrm{d}t. \tag{24}$$

The new $\mathbf{M}_c$, $\mathbf{C}_c$ and $\mathbf{K}_c$ matrices now include the mechanical and electrical subsystems. The resulting linear system of equations can be solved using the same steady-state methods as with the mechanical system. In this study, the primary focus is on the torsional response, which is solved directly from these combined matrices using Eq. (18). When the proposed coupled model is used, the same equation can be used to calculate the response of purely mechanical and combined linearized electromechanical systems.

The natural frequencies of the combined electromechanical system are given as the absolute values of the eigenvalues of the system matrix $\mathbf{A}_c$. The mode shapes associated with these eigenvalues are the eigenvectors of the same system matrix. It is evident from this formulation, that the eigenvalues of the combined system are operating point dependent. If a symbolic solution to the eigenfrequencies is preferred instead of the eigenvalues of the system matrix, the transfer function formulation in Fig. 3 can be applied. Derivation of the symbolic solution for the closed-loop poles of the coupled system is presented in Appendix A.

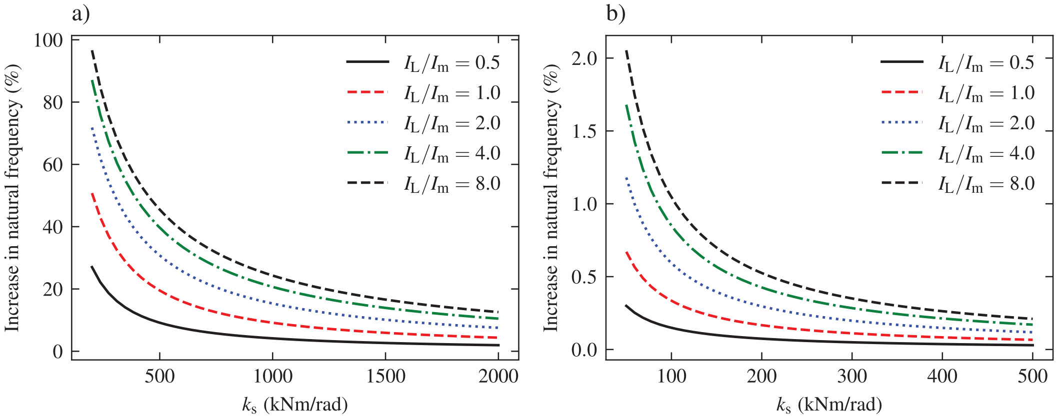

Fig. 7. Comparison of the torsional natural frequency of the coupled two-mass model with the purely mechanical model. (a) the 3.7 MW and (b) the 37 kW induction motor models in rated operating point, using different ratios of load and motor inertia I_L/I_m and varying the shaft stiffness k_s.

Table 2
Mechanical parameters for the two induction motor driven systems.

Parameter	Symbol	Value		Unit
		Motor 37 kW	Motor 3.7 MW	
Shaft stiffness	k_s	10	835	kN/rad
Shaft internal damping	c_s	4	2000	N m/rad^2
Motor external damping	d_m	0	100	N m/rad^2
Load inertia	I_L	0.512	1758.4	kg m^2

5. Results

Coupled electromechanical torsional vibrations are investigated. The derived linearized model is compared with established non-linear simulations. First, the influence of the electromagnetic effect is studied on the natural frequencies on a two-mass mechanical system. Next, the torsional vibration response of the linearized electromechanical models with two-mass mechanics are compared to steady-state responses calculated with time-stepping simulation. An application example of a compressor powertrain is presented to highlight the importance of including the feedback dynamics in the analysis and shows the extension to a more complex mechanical system. Finally, the stability of the coupled system is analyzed and compared with experimental measurements.

5.1. Influence of the electromagnetic effect on torsional eigenfrequencies

The influence of the electromagnetic coupling is investigated on the two-mass model (Fig. 5). The calculations are based on the 37 kW and 3.7 MW induction motors, parameters given in Table 1. The mechanical parameters of the models are varied to cover multiple cases. The eigenfrequencies of the system are calculated using a purely mechanical model, and compared to ones of the system which is coupled with the electrical subsystem. The increase in natural frequency due to the magnetic stiffness is considered in the rated operating point of each motor. The natural frequencies of the coupled system are computed from the eigenvalues of the system matrix $\mathbf{A}_c$ assembled as shown in Eq. (22). The natural frequencies could be equivalently computed from the symbolic solution presented in Appendix A. Following this parameter varying analysis, representative examples are chosen for a further study of the operating point dependence of the solutions.

Fig. 7 depicts how the increase in torsional natural frequency of the two mass model is dependent on the mechanical parameters. In general, these results are consistent with previous findings, where it has been shown, that the electromagnetic stiffness acts as an additional external magnetic spring constant on the mechanical system. The relative influence of the electromagnetic stiffness is inversely proportional to the shaft stiffness k_s, regardless of the load inertia I_L. The relative increase in torsional natural frequencies is by an order of magnitude larger in the typical mechanical parameter scale of the larger 3.7 MW induction motor. According to the present analysis, the influence on the natural frequencies is negligible in most mechanical configurations which can be considered to be in typical range for applications employing 37 kW induction motors.

To study the frequency dependence of the em-effect, a Campbell diagram (Fig. 8) is calculated for each motor in a two-mass mechanical configuration with the parameters given in Table 2. The same mechanical parameters used in the Campbell diagrams are later used in the next section for the response calculations. The electrical parameters are given in Table 1. The diagrams show the influence of the operating point stator frequency on the eigenfrequencies. The eigenfrequencies are normalized by the purely mechanical torsional eigenfrequency. Mode veering of the coupled electromechanical models is seen at intersections of the

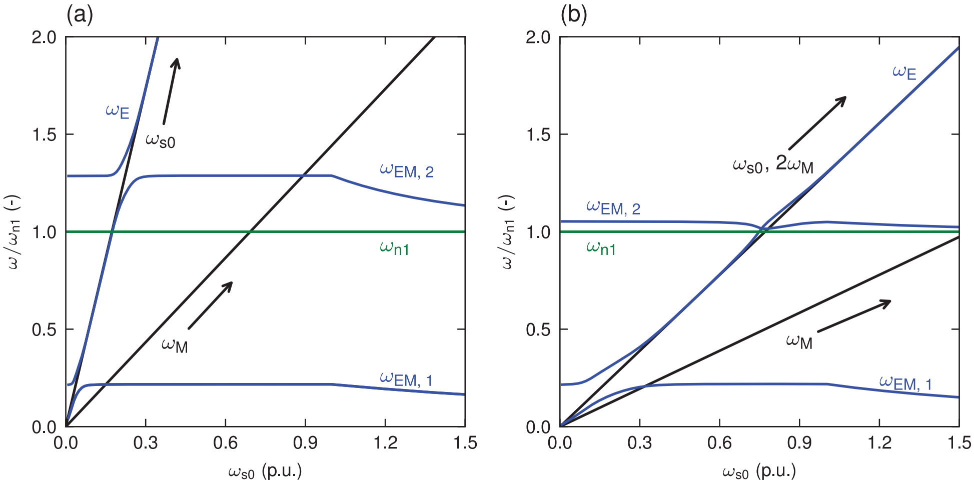

Fig. 8. Resonance interference diagram of the coupled electromechanical two-mass system in no-load ($\tau_{m0} = 0$) condition. (a) 3.7 MW induction motor, (b) 37 kW induction motor. The EM-influence increases the frequency of the rigid body mode as well as the frequency of the first elastic mode. The natural frequencies of the combined electromechanical modes decrease in the field weakening region ($\omega_{s0} > 1$).

eigenfrequencies. The presence of mode veering indicates, that the mechanical eigenmodes have become coupled with the electrical eigenmodes. While the eigenfrequencies remain mostly independent of the rotating speed, they show a decreasing trend in the field-weakening region, (as $\omega_{s0} > 1$). This effect is due to the decrease in the operating point stator flux linkage.

5.2. Response calculation in variable-speed two-mass mechanical system

Torsional vibration responses of the two motor systems are considered. The responses are calculated using two methods, with the proposed linearization approach, and with time-stepping simulations in the steady-state. The mechanical and electrical parameters of the investigated cases are the same as in the Campbell diagrams calculated in the previous section (c.f. Fig. 8). In the torsional response, the electromagnetic effect is manifested as an increase of the mechanical eigenfrequencies, as well as a changes in the vibration amplitudes. In general, the electromagnetic effects increase the damping of the system, as energy is dissipated from the induced currents in the stator coils through resistive losses.

Simulation software based on verified models was established. Motulator [43], an open-source Python electric drive simulation software was used to implement the control and electrical subsystem simulations. An open-source torsional vibration library, openTorsion, was used to implement the mechanical subsystem. The mechanical and electrical equations are solved together within the motulator simulator according to the parameter interfaces shown in Fig. 3. The derivatives of the coupled model are calculated for both subsystems at each time-step. The control system is solved in discrete-time, while the electrical and mechanical subsystems are solved in continuous time. The coupled non-linear simulation model can be used for analysis of transient phenomena as well as steady-state vibrations. This interconnected simulation approach bears resemblance to the model established in [29].

All steady-state response simulations follow the same procedure. The simulation starts from standstill and the motor voltage is increased until the speed set-point is reached. The voltage increase is rate-limited. When the acceleration has ended, the load torque is applied as a step increase which is superimposed on the harmonic excitation. For simplicity, the simulations presented in this section include only one frequency component, enabling the harmonic response to be accurately retrieved from the simulation output. The torsional excitation is applied as noted in Eq. (16), but different frequencies and amplitudes are applied in the two cases. For this analysis, the vibration amplitudes are chosen so that vibration responses would be within realistic limits in actual machinery. The absolute vibration amplitudes are however not that important, since the main focus is on the relative amplitudes. For the 37 kW motor driven model, an excitation at twice the rotating frequency is applied with constant amplitude $X = 0.1\tau_{\text{rated}}$. In the 3.7 MW motor case, the excitation frequency equal to the rotating frequency, and the amplitude is proportional to the square of the rotating frequency, $X = 0.2\tau_{\text{rated}}\omega_M^2/\omega_{\text{rated}}^2$.

Fig. 9 displays the responses calculated for the 3.7 MW induction motor coupled with the two-mass mechanical system. Inclusion of the electromagnetic effects in the model causes a shift in the torsional response peaks. The elastic mode becomes coupled with the electrical subsystem and increases in frequency. In the lower rotating speeds, the EM-influence causes the so-called rigid body mode resonance to appear in the response. This resonance intersection is also confirmed from the previously discussed Campbell diagram (Fig. 8). The simulated steady-state simulation responses are in good alignment with the analytical solution. It should be noted, that the computation time required for the simulation results are orders of magnitude larger compared to the computation needed for the analytic solutions.

Response calculations of the coupled two-mass model for the 37 kW motor are shown in Fig. 10. The predominant response peaks are seen at half the eigenfrequency, since the applied excitation frequency is twice the rotating frequency. The responses are

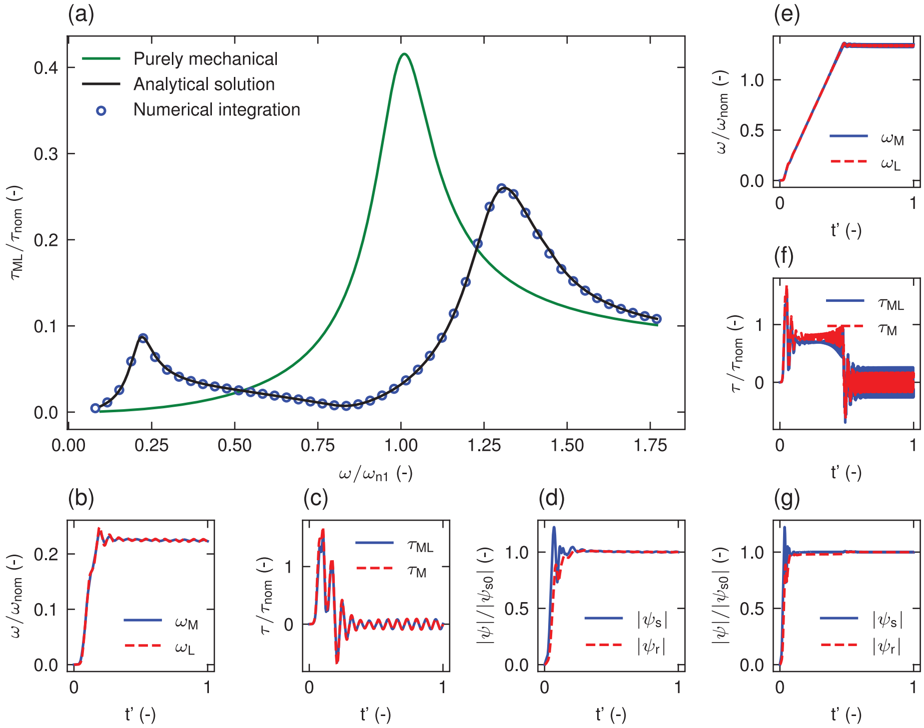

Fig. 9. (a) Comparison of simulation results and the linearized model in an example calculation for the 3.7 MW motor. Panels (b–d) show the simulation at the first resonance peak and panels (e–g) in the second peak. The proposed analytic approximation produces the same result as the time-stepping simulation performed using numerical integration.

calculated in three loading cases: no-load $\tau_{m0} = 0$, rated torque $\tau_{m0} = \tau_{rated}$, and rated regenerative torque $\tau_{m0} = -\tau_{rated}$. In this analysis, the operating point torque does not significantly alter the frequency of the response peak for the elastic mode, but has an effect on the peak amplitude. The load torque affects the slip of the motor, which in turn modifies the magnetic stiffness and damping properties of the electrical subsystem. In this case, the overall system damping decreases with the steady-state motor torque. Again, the simulated steady-state responses align well with the linearized analytical solution, however, at low rotating speeds, there is visible discrepancy between the simulations and the analytic solution. This is expected, since with the relatively high excitation amplitude at such a low frequency, the operating point does not remain constant, which compromises the linearization assumption. Induction motors are however not typically designed for extended operation at such low operating speeds.

These results indicate, that the assumption made in the small-signal linearization do not greatly affect the calculation of the steady-state response. In the presented analyses vibration amplitude is high or moderate in comparison to the rated torque. The torsional response calculations also confirm the presence of the resonances anticipated from the Campbell diagrams calculated in the previous section. The coupled analysis approach could be a valuable option for powertrain designers screening potential issues with EM-influence, as has also been suggested in the earlier literature [13,31]. The extent of these electromagnetic stiffness and damping properties could also have been estimated using the electromagnetic stiffness and damping derived from the mechanical impedance (c.f. Eq. (13)), however, this approach would require iteration to compute the eigenfrequencies, which is not required in the proposed approach.

5.3. Analysis of a motor-driven compressor

A motor driven compressor powertrain is used as an example of the proposed modeling workflow. The motor and control system is based on the 3.7 MW induction motor, identical to the one analyzed in the earlier sections. Parameters of the compressor model are based on an industrial example and the equivalent circuit parameters have been identified from electromagnetic finite element analysis by the motor manufacturer [9]. The purely mechanical model is coupled with the small-signal linearized equivalent circuit and control system models. Free vibrations of the coupled system are investigated and the Campbell diagram is calculated. Finally, the steady-state forced response is calculated in all operating speeds of the compressor train. Small-signal unstable regions originating from the coupling of the mechanics and the control system are found from analysis of the eigenvalues. The calculations are verified with time-stepping simulations.

The mechanical compressor train model consists of 11 lumped-mass elements connected with massless-elastic spring elements, as shown in Fig. 11. The model is formed by matching the topology, and tuning the mass and stiffness properties to match the

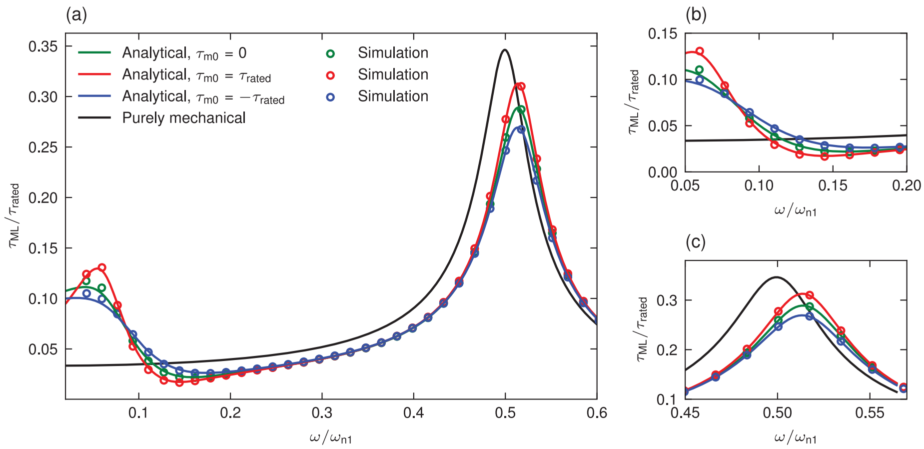

Fig. 10. Comparison of simulation results and the analytical model in an example calculation for the 37 kW motor (a). Closeup of the resonance peaks (b–c). The model consists of the two-mass mechanical system and the equivalent circuit model. Excitation at twice the rotating frequency is applied on the load mass. The analysis is performed in three different loading conditions. The analytic approximation produces the same result as the time-stepping simulation.

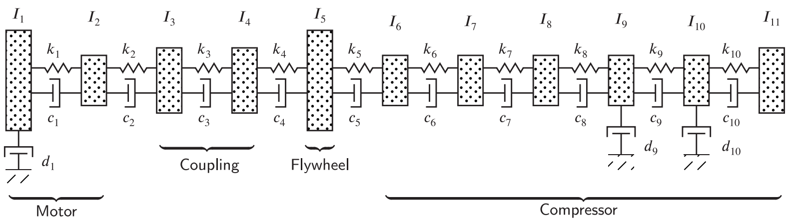

Fig. 11. The compressor train model consists of the electric motor, coupling, flywheel and the compressor cylinders. The parameters of the model are given in the Appendix A.

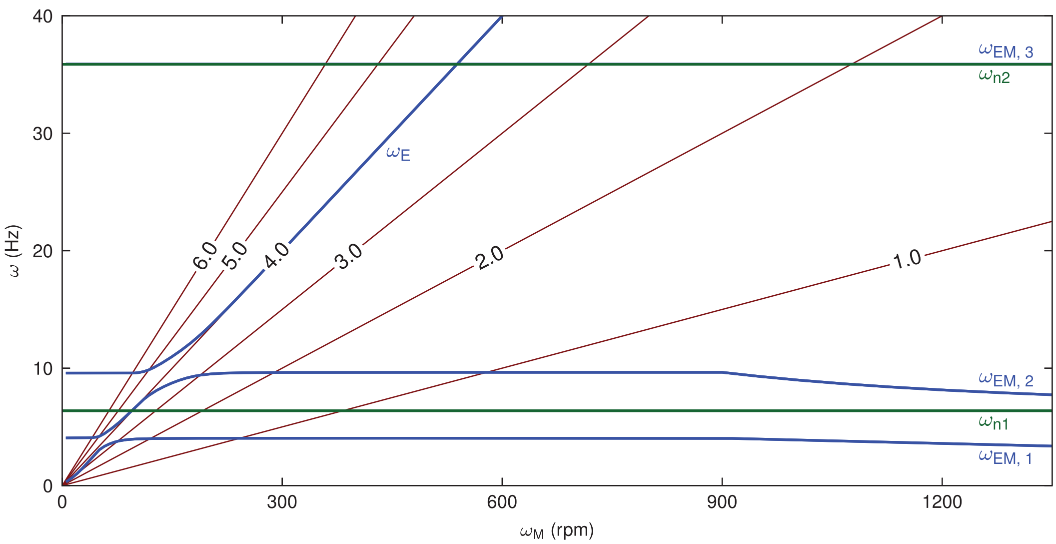

Fig. 12. Resonance interference diagram of the compressor system. Largest difference between the purely mechanical and coupled model is seen in the first torsional mode, which increases up to 51%.

lowest natural frequencies of the model to the one considered in [9]. Internal viscous damping is included in all shafts to achieve realistic damping ratios for the torsional modes. Additionally, external viscous damping is added to the motor and cylinder nodes. The complete list of mechanical parameters are given in Appendix B.

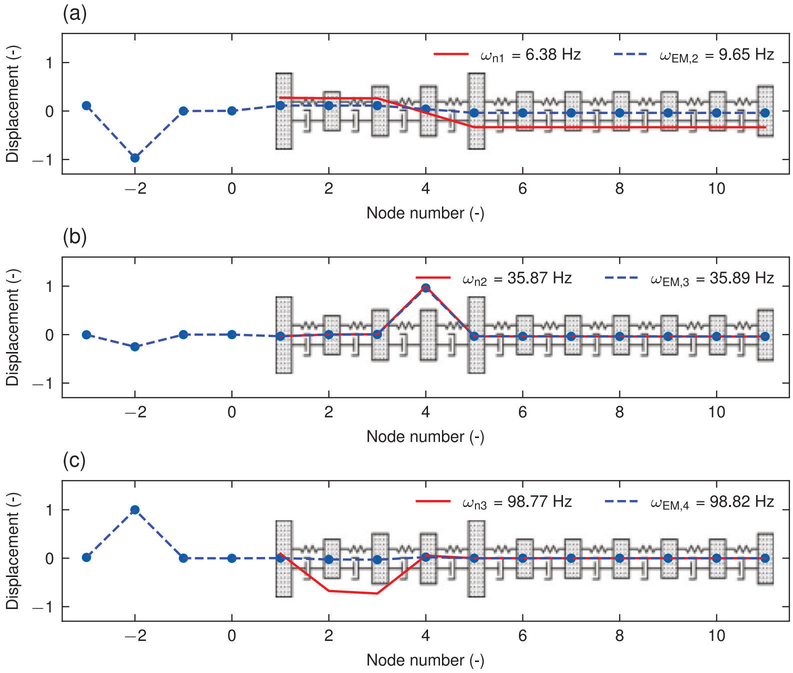

Fig. 13. First three elastic torsional modes of the compressor train (a–c). Degrees of freedom associated with the electric motor are denoted with indexes 0 to −3.

In the compressor systems, major excitations originate from the compression cycle at integer multiples of the rotating speed. Analysis of the forced response was performed by applying a harmonic excitation where the excitation frequencies are multiples of the fundamental frequency, i.e., the rotating speed of the compressor. The same excitation is used in the mechanical model for comparison. The excitation model consists of the first 24 harmonics of the rotating frequency. The amplitude of the harmonic components is assumed to decay at higher frequencies, in this model, harmonic amplitude is divided by its order number. Since the force at each two compressor cylinders act in opposite phase relative to each other, the excitation is applied to both cylinder nodes with half a rotation phase difference.

The linearized combined electromechanical model is assembled following Eq. (22). The necessary operating point quantities are calculated from the steady-state equations Eqs. (10)–(11). Calculating the eigenvalues at all operating points yields the Campbell diagram, seen in Fig. 12. The compressor excitations are shown in the diagram up to the sixth order. The new mode introduced by the electromagnetic system appears at frequencies below the first torsional natural frequency. The first torsional eigenfrequency of the purely mechanical model is also shifted to higher frequency due to the EM-effect. In the field weakening region, at speed over 900 rpm, the eigenfrequencies drop along with the stator flux linkage. The eigenvectors of the lowest elastic modes calculated at the rated operating point are shown in Fig. 13. It is noted, that the two first torsional eigenmodes become coupled with the electromagnetic subsystem. As expected, the EM-effect is negligible in higher order torsional modes, as these modes do not have relative motion in the rotor of the induction motor. It was found in the eigenvalue analysis, that unstable poles are present in the coupled system in operating speeds from 130 rpm to 190 rpm. This unstable speed-range is dependent on the total inertia of the drivetrain [23].

The torsional vibration response was calculated using the coupled model and Eq. (18). The responses are calculated at compressor operating speeds ranging from standstill to 900 rpm. The same responses are also calculated with non-linear time-stepping simulation. Results from the non-linear simulations and the analytic solutions are shown in Fig. 14. The purely mechanical response is also shown for reference. As predicted by the eigenvalue analysis, the resonance speed of the lowest flexible mode is shifted to a higher frequency. In turn, the new vibration mode introduced by the EM-effect, visible at approximately 120 rpm, becomes the most important resonance peak of the coupled system. Unstable vibrations are present in the simulations at low to mid rotating speeds. These unstable speeds match with the speeds predicted by the eigenvalue analysis. Simulation results also differ slightly from the analytical results near the unstable region, this might be due to the system not having enough time to reach steady-state at such a low damping. Eq. (20) defines the response as a sum of the absolute values of the vibratory torque components. This calculation corresponds to the worst-case and thus overestimates the peak-to-peak vibrations of responses with multiple frequency components. Thus, the maximum peak-to-peak value within 30 s is extracted from the analytic solution for comparison with the non-linear response.

Analysis of these results reveal, that the EM-effects are significant in the case of this compressor train. Conventional means of torsional vibration analysis, i.e., the purely mechanical model, could lead to large error in identification of the resonance speeds.

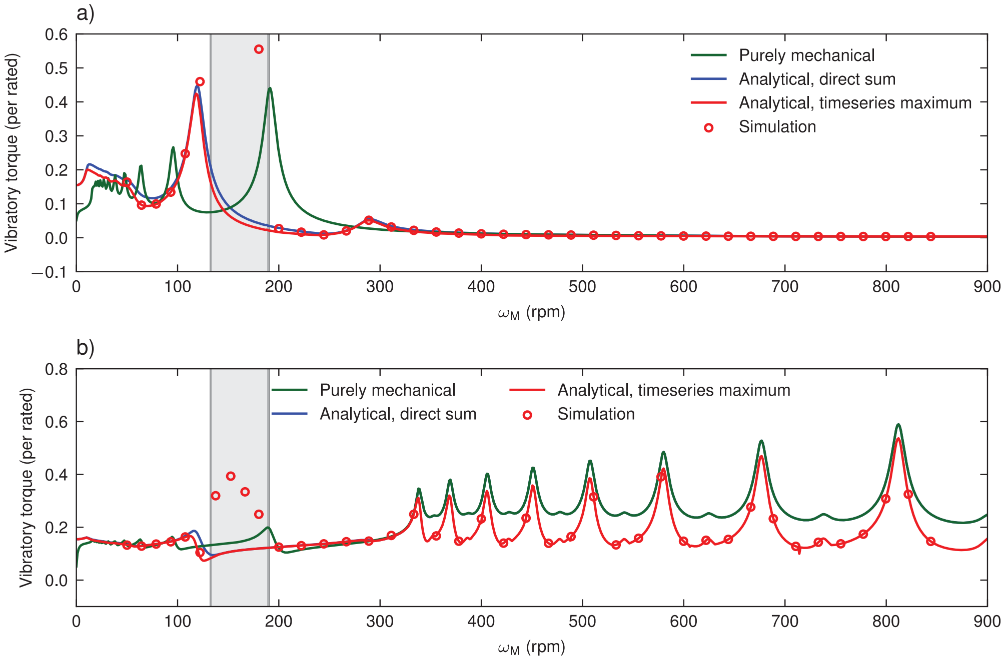

Fig. 14. Steady state vibratory torque response of the compressor powertrain. The vibratory torque is shown at two shafts, at the flexible coupling (a) and right beyond the flywheel (b). Unstable operating speeds predicted by the linearized model are highlighted with a gray background.

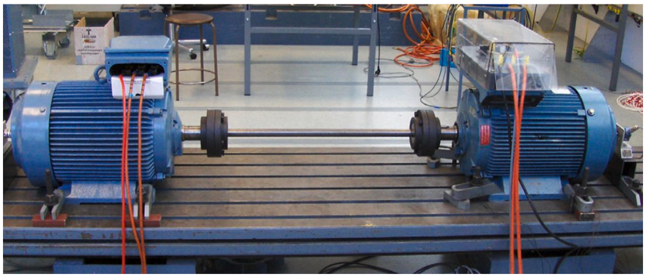

Fig. 15. Two almost identical 37 kW induction motors connected by a flexible shaft [10].

The importance of considering these effects is highlighted in the vibratory torque of the coupling, where the resonance speed differs greatly in the coupled case. The EM-effects are negligible in the operating speed region of the compressor system from 450 rpm to 900 rpm. This occurs because the flexible coupling and flywheel together function as a low-pass filter, preventing high-frequency vibrations from transferring from the compressor side to the motor. This result indicates that modeling the electrical system is more important if critical locations are near the motor, such as flexible couplings, and the EM-effect should be considered in selection of the coupling. In the present case, the coupling choice could be re-considered to mitigate the resonance effects caused by the shift of the natural frequency due to the electromagnetic effect.

5.4. Comparison with experiments

To verify the unstable torsional vibrations predicted by the model, measurements of the 37 kW motor reported in [10] are considered. The measurement setup, shown in Fig. 15, includes two almost identical 37 kW motors connected back to back with a flexible shaft. Pulse tachometers were used to measure the torsional vibrations. The mechanical torsional natural frequency was designed to be 36 Hz. The corresponding stiffness in the two-mass model is 6.55 kN m and the two inertias equal to the inertia of the rotor. The measured natural frequency varied from 39.25 to 39.75 Hz. The motors were supplied from a 750 kVA synchronous generator and V/Hz control was used to maintain approximately constant flux.

Fig. 16 shows the root loci of the combined electromechanical system as the supply frequency is increased. Zero mechanical damping is assumed corresponding to the worst case scenario. As in the experiments, the operating points are in no-load condition. The natural frequency corresponding to the first torsional mode seen in the root locus plot is also shown in the resonance interference

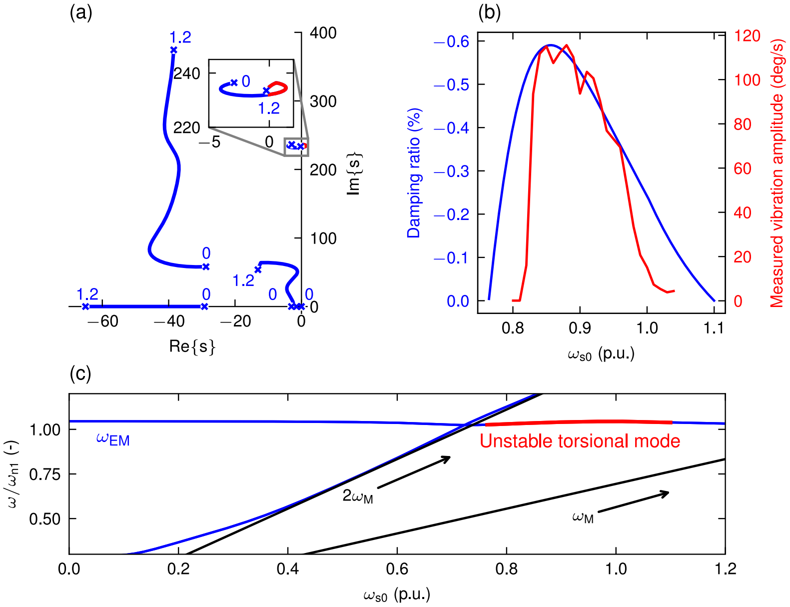

Fig. 16. Unstable torsional mode below and just above the rated supply frequency. (a) Shows the root locus plot of the coupled system as the operating point stator angular frequency varies from 0 to 1.2 (p.u.), predicted and measured range on unstable vibrations (b), the same unstable speed region is seen in the Campbell diagram (c). The measured self-excited limit cycle vibrations reported by [10] closely match the unstable torsional mode of the electromechanical system.

diagram. These self-excited unstable torsional vibrations do not originate from a resonance, but from the coupled electromechanical instability of the elastic torsional mode. Instability of the torsional mode is manifested as limit cycle vibrations at the coupled natural frequency. As the supply frequency increases, the torsional instability occurs at frequency right above the two-times fundamental frequency resonance. According to the measurements, this resonance is expected at supply frequency approximately $\omega_{s0} = 39.5$ Hz, while the measurements unstable vibrations occur in the input frequency range 40 Hz to 50 Hz. The predicted range of instability damping ratio of the coupled linearized model is similar to the measured phenomenon. The model slightly overestimates the range of instability, as it assumes no mechanical damping. Increasing the mechanical damping shifts the poles towards the negative real axis. At sufficient level of damping, no instability can occur.

The torsional instability is caused by the feedback mechanism formed between the electrical and mechanical subsystems. The torsional oscillations of the motor induce currents in the stator coils, causing an additional harmonic in the electromagnetic torque. At certain frequency range, the phase of the torque harmonic can be such that this feedback mechanism supplies power to the torsional mode. If the mechanical damping of the torsional mode is low, instability of the torsional mode is possible. To avoid the risk of instability, several means can be considered. The control system can be modified to prevent the phase of the torque to feed power to the torsional mode [27]. The mechanical natural frequency can be designed to not be in the frequency range where the risk of instability is present. Mechanical damping can be increased with e.g., with choice of coupling or implementing a torsional damper.

6. Conclusions

Linearization approach for torsional response calculation of electric motor driven machines was considered, reaching the following conclusions.

1. Harmonic solution for the interconnected torsional forced response problem comprising of the mechanical, electrical and control system models can be derived analytically. The proposed analysis framework provides a rapid evaluation tool for steady-state vibrations problems with electromagnetic coupling, including forced response and stability analyses.
2. The magnetic stiffness and damping introduced by the drive system are dependent on the motor, control system and operating point. Omitting these effects by considering the torque produced by the electric motor as an input without the feedback mechanism may lead to significant errors in calculated responses. The proposed modeling framework is an effective way for correctly accounting for the operating point. In the application example of a compressor driven powertrain, the increase in the frequency of the lowest elastic mode is up to 51%.
3. Self-excited unstable vibrations can originate from the feedback dynamics of the coupled system. Best known instabilities are caused by the interaction control system influenced by the total inertia, as seen in the case of the mid-speed instability in the

analysis of the compressor train. In addition to the well-known unstable mid-speed region, an additional torsional instability is possible due to coupling between the electrical subsystem and an elastic torsional mode. These unstable torsional vibrations arising in the vicinity of a harmonic resonance could be mischaracterized as resonant vibrations. The risk of instability is present especially in drivetrains, where the natural frequency is slightly below the rated supply frequency and mechanical damping is low.

CRediT authorship contribution statement

Sampo Laine: Writing – original draft, Visualization, Validation, Software, Methodology, Investigation, Funding acquisition, Formal analysis, Conceptualization. **Urho Hakonen:** Writing – review & editing, Visualization, Software, Investigation. **Hannu Hartikainen:** Writing – review & editing, Methodology, Conceptualization. **Raine Viitala:** Writing – review & editing, Supervision, Funding acquisition.

Declaration of competing interest

The authors declare that they have no known competing financial interests or personal relationships that could have appeared to influence the work reported in this paper.

Appendix A. Symbolic solution for the closed loop poles

The transfer function $Z_{\mathrm{M}}(s)$ from motor speed to electromagnetic torque can be derived from the small-signal T-equivalent circuit model. At a given operating point, the single-input single-output small-signal model can be written as

$$\frac{d}{dt}\mathbf{x} = \mathbf{A}(s)\delta\mathbf{x} + \mathbf{b}\delta\omega_M, \tag{25}$$

$$\delta\tau_m = \mathbf{c}\mathbf{x}, \tag{26}$$

where s is the Laplace variable.

The matrix $\mathbf{A}$

$$\mathbf{A}(s) = \begin{bmatrix} (R_{\mathrm{s}} + sL_{\mathrm{s}})\mathbf{I} + \omega_{\mathrm{s0}}L_{\mathrm{s}}\mathbf{J} & sL_{\mathrm{m}}\mathbf{I} + \omega_{\mathrm{s0}}L_{\mathrm{m}}\mathbf{J} \\ sL_{\mathrm{m}}\mathbf{I} + (\omega_{\mathrm{s0}} - \omega_{\mathrm{s0}})L_{\mathrm{m}}\mathbf{J} & (R_{\mathrm{r}} + sL_{\mathrm{r}})\mathbf{I} + (\omega_{\mathrm{s0}} - \omega_{\mathrm{m0}})L_{\mathrm{r}}\mathbf{J} \end{bmatrix}, \tag{27}$$

the vector $\mathbf{b}$

$$\mathbf{b} = \begin{bmatrix} 0 & 0 & -p(L_{\mathrm{r}}i_{\mathrm{rq0}} + L_m i_{\mathrm{sq0}}) & p(L_{\mathrm{m}}i_{\mathrm{sd0}} + L_{\mathrm{r}}i_{\mathrm{rd0}}) \end{bmatrix}^{\mathrm{T}}, \tag{28}$$

and the vector $\mathbf{c}$

$$\mathbf{c} = -\frac{3pL_m}{2}\begin{bmatrix} i_{\mathrm{rq0}} & -i_{\mathrm{rd0}} & -i_{\mathrm{sq0}} & i_{\mathrm{sd0}} \end{bmatrix}. \tag{29}$$

The frequency response from rotor speed to electromagnetic torque is then solved as

$$Z_{\mathrm{M}}(s) = \frac{\delta\tau_{\mathrm{m}}(s)}{\delta\omega_{\mathrm{M}}(s)} = \mathbf{c}\mathbf{A}^{-1}(s)\mathbf{b}. \tag{30}$$

For a two-mass mechanical system, the transfer function is

$$G_{\mathrm{M}}(s) = \frac{1}{Js}\frac{J_{\mathrm{L}}s^2 + C_{\mathrm{S}}s + K_{\mathrm{S}}}{(J_{\mathrm{M}}J_{\mathrm{L}}/J)s^2 + C_{\mathrm{S}}s + K_{\mathrm{S}}}. \tag{31}$$

The closed-loop poles are obtained by solving

$$1 + Z_{\mathrm{M}}(s)G_{\mathrm{M}}(s) = 0 \tag{32}$$

Symbolic solution for the transfer function Z_{M} can be directly calculated using Eq. (30), this solution is however long and more conveniently presented by substituting the numerical values. In the rated operating point, the transfer function equates to

$$Z_{\mathrm{M,\ rated}}(s) = \frac{-1280s^3 - 87700s^2 - 1.27\cdot 10^8 s - 3.55\cdot 10^9}{s^4 + 133s^3 + 103300s^2 + 5.75\cdot 10^6 s + 9\cdot 10^7} \tag{33}$$

The symbolic solution for the closed-loop poles follows directly from substituting Eqs. (31) and (33) to Eq. (32) and solving.

Appendix B. Parameters of the compressor train model

Mechanical parameters of the compressor train model are given in Table 3.

Table 3
Parameters of the compressor mechanics.

Component	Node number n –	Inertia I_n kg m^2	Stiffness k_n MN m/rad	Internal damping c_n kN m/rad^2	External damping d_n kN m s/rad
Motor 1	1	211.4	9.775	2.0	0.1
Motor 2	2	8.3	100	0.4	0
Coupling 1	3	20	0.35	0.4	0
Coupling 2	4	14	0.35	0.4	0
Flywheel	5	150	100	0.4	0
Compressor 1	6	5	85	1.0	0
Compressor 2	7	6	85	1.0	0
Compressor 3	8	6	85	2.0	0
Compressor 4	9	6	85	2.0	0.1
Compressor 5	10	5	85	2.0	0.1
Compressor 6	11	15	100	1.0	0

Data availability

Data will be made available on request.

References

[1] J. Song-Manguelle, S. Schroder, T. Geyer, G. Ekemb, J.-M. Nyobe-Yome, Prediction of mechanical shaft failures due to pulsating torques of variable-frequency drives, IEEE Trans. Ind. Appl. 46 (5) (2010) 1979–1988, http://dx.doi.org/10.1109/TIA.2010.2057397.

[2] M. Bruha, Z. Peroutka, Torsional vibration in large variable speed drive systems: Origin and mitigation methods, in: 2015 17th European Conference on Power Electronics and Applications, EPE'15 ECCE-Europe, 2015, pp. 1–10, http://dx.doi.org/10.1109/EPE.2015.7309169.

[3] M. Mauri, M. Rossi, M. Bruha, Generation of torsional excitation in a variable-speed-drive system, in: 2016 International Symposium on Power Electronics, Electrical Drives, Automation and Motion, SPEEDAM, IEEE, Capri, Italy, 2016, pp. 516–521, http://dx.doi.org/10.1109/SPEEDAM.2016.7525862.

[4] K. ElShawarby, R. Perini, G.M. Foglia, A. di Gerlando, M. Rossi, F.C. Dezza, A practical solution for torsional vibrations evasion in variable speed drives, in: IECON 2019 - 45th Annual Conference of the IEEE Industrial Electronics Society, IEEE, Lisbon, Portugal, 2019, pp. 4439–4444, http://dx.doi.org/10.1109/IECON.2019.8927620.

[5] J. Sopanen, V. Ruuskanen, J. Nerg, J. Pyrhonen, Dynamic torque analysis of a wind turbine drive train including a direct-driven permanent-magnet generator, IEEE Trans. Ind. Electron. 58 (9) (2011) 3859–3867, http://dx.doi.org/10.1109/TIE.2010.2087301.

[6] B. Ooi, T.-S. Low, Electromechanical spring stiffness from the small perturbation linearized equations of generalized machine theory, IEEE Trans. Energy Convers. 5 (2) (1990) 374–379, http://dx.doi.org/10.1109/60.107235.

[7] A. Tabesh, R. Iravani, Frequency-response analysis of torsional dynamics, IEEE Trans. Power Syst. 19 (3) (2004) 1430–1437, http://dx.doi.org/10.1109/TPWRS.2004.831684.

[8] A. Arkkio, T.P. Holopainen, Space-vector models for torsional vibration of cage induction motors, IEEE Trans. Ind. Appl. 52 (4) (2016) 2988–2995, http://dx.doi.org/10.1109/TIA.2016.2547361.

[9] T.P. Holopainen, J. Roivainen, T. Ryyppö, Digital twin of induction motors for torsional vibration analysis of electrical drive trains, in: 12th International Conference on Vibrations in Rotating Machinery, 2020, p. 12.

[10] A.-K. Repo, P. Rasilo, A. Niemenmaa, A. Arkkio, Identification of electromagnetic torque model for induction machines with numerical magnetic field solution, IEEE Trans. Magn. 44 (6) (2008) 1586–1589, http://dx.doi.org/10.1109/TMAG.2007.916143.

[11] T. Feese, A. Kokot, Electromagnetic effects on the torsional natural frequencies of an induction motor driven reciprocating compressor with a soft coupling, in: 45th Turbomachinery & 32nd Pump Symposia, Houston, Texas, September, 2016, p. 22.

[12] O. Thorsen, M. Dalva, Combined electrical and mechanical model of electric submersible pumps, IEEE Trans. Ind. Appl. 37 (2) (2001) 541–547, http://dx.doi.org/10.1109/28.913720.

[13] S. Zhang, J. Wei, Z. Xu, B. Tang, R. Niu, Research on the influence of system parameters on the electromechanical dynamics of a large wind turbine drivetrain, Energy Rep. 7 (2021) 7835–7851, http://dx.doi.org/10.1016/j.egyr.2021.11.020.

[14] X. Shi, D. Sun, Y. Kan, J. Zhou, Y. You, Dynamic characteristics of a new coupled planetary transmission under unsteady conditions, J. Braz. Soc. Mech. Sci. Eng. 42 (6) (2020) 280, http://dx.doi.org/10.1007/s40430-020-02371-w.

[15] D. Wang, F. Yang, X. Jiang, S. Shi, S. Ma, Electromechanical coupling dynamic characteristics of differential speed regulation system considering inverter harmonics under variable operating conditions, IEEE Access 10 (2022) 12057–12069, http://dx.doi.org/10.1109/ACCESS.2022.3143537.

[16] L. Han, D. Wang, F. Yang, W. He, Vibration characteristics of the dual electric propulsion system of vessels under electromechanical coupling excitation, Machines 10 (6) (2022) 449, http://dx.doi.org/10.3390/machines10060449.

[17] B.E. Yousfi, A. Soualhi, K. Medjaher, F. Guillet, Electromechanical modeling of a motor–gearbox system for local gear tooth faults detection, Mech. Syst. Signal Process. 166 (2022) 108435, http://dx.doi.org/10.1016/j.ymssp.2021.108435.

[18] Z. Ziwei, C. Zaigang, S. Maksym, W. Peter, W. Qing, Z. Wanming, C. Cole, Dynamic performance of locomotive electric drive system under excitation from gear transmission and wheel-rail interaction, Veh. Syst. Dyn. 60 (5) (2022) 1806–1828, http://dx.doi.org/10.1080/00423114.2021.1876887.

[19] S. Saarakkala, Identification and Speed Control Design of Resonating Mechanical Systems in Electric Drives (Doctoral thesis), School of Electrical Engineering, 2014, URL http://urn.fi/URN:ISBN:978-952-60-5827-6.

[20] W. Pawlus, M.R. Hansen, M. Choux, G. Hovland, Mitigation of fatigue damage and vibration severity of electric drivetrains by systematic selection of motion profiles, IEEE/ASME Trans. Mechatronics 21 (6) (2016) 2870–2880, http://dx.doi.org/10.1109/TMECH.2016.2573587.

[21] M. Rossi, K. Elshawarby, M. Bruha, M. Mauri, M. Carmeli, F. Castelli-Dezza, Performance evaluation methods for VSD control systems affected by torsional vibrations: Sensitivity and energetic analyses, in: 2019 International Conference on Clean Electrical Power, ICCEP, IEEE, Otranto, Italy, 2019, pp. 605–610, http://dx.doi.org/10.1109/ICCEP.2019.8890227.

[22] M. Rossi, M.S. Carmeli, M. Mauri, Adjustable speed control and damping analysis of torsional vibrations in VSD compressor systems, Machines 9 (12) (2021) 374, http://dx.doi.org/10.3390/machines9120374.

[23] M. Hinkkanen, L. Tiitinen, E. Mölsä, L. Harnefors, On the stability of volts-per-hertz control for induction motors, IEEE J. Emerg. Sel. Top. Power Electron. 10 (2) (2022) 1609–1618, http://dx.doi.org/10.1109/JESTPE.2021.3060583.

[24] S. Mishra, A.B. Palazzolo, X. Han, Y. Li, C. Kulhanek, Torsional vibrations in open loop volts hertz variable frequency drive induction motor driven mechanical systems, in: 2020 IEEE Texas Power and Energy Conference, TPEC, IEEE, College Station, TX, USA, 2020, pp. 1–6, http://dx.doi.org/10.1109/TPEC48276.2020.9042586.

[25] G.-J. Jo, J.-W. Choi, Rotor field-oriented v / f drive system implementation with oscillation suppression compensator in induction motors, IEEE J. Emerg. Sel. Top. Power Electron. 9 (3) (2021) 2745–2758, http://dx.doi.org/10.1109/JESTPE.2020.2999973.

[26] L. Carbone, S. Cosso, K. Kumar, M. Marchesoni, M. Passalacqua, L. Vaccaro, Stability analysis of open-loop V/Hz controlled asynchronous machines and two novel mitigation strategies for oscillations suppression, Energies 15 (4) (2022) 1404, http://dx.doi.org/10.3390/en15041404.

[27] L. Tiitinen, M. Hinkkanen, L. Harnefors, Stable and passive observer-based V/Hz control for induction motors, in: 2022 IEEE Energy Conversion Congress and Exposition, ECCE, 2022, pp. 1–8, http://dx.doi.org/10.1109/ECCE50734.2022.9948057.

[28] W. Bai, D. Qin, Y. Wang, T.C. Lim, Dynamic characteristic of electromechanical coupling effects in motor-gear system, J. Sound Vib. 423 (2018) 50–64, http://dx.doi.org/10.1016/j.jsv.2018.02.033.

[29] K. Liu, W. Wu, S. Yuan, G. Lu, X. Chen, Modal characteristics of electric vehicle powertrain considering electromagnetic effect, J. Sound Vib. 530 (2022) 116972, http://dx.doi.org/10.1016/j.jsv.2022.116972.

[30] N. Feki, G. Clerc, P. Velex, An integrated electro-mechanical model of motor-gear units—Applications to tooth fault detection by electric measurements, Mech. Syst. Signal Process. 29 (2012) 377–390, http://dx.doi.org/10.1016/j.ymssp.2011.10.014.

[31] Y. Yi, D. Qin, C. Liu, Investigation of electromechanical coupling vibration characteristics of an electric drive multistage gear system, Mech. Mach. Theory 121 (2018) 446–459, http://dx.doi.org/10.1016/j.mechmachtheory.2017.11.011.

[32] J. Tan, Study on the dynamic modeling and natural characteristics of wind turbine drivetrain considering electromagnetic stiffness, Mech. Mach. Theory (2019) 21.

[33] A. Tabesh, R. Iravani, On the application of the complex torque coefficients method to the analysis of torsional dynamics, IEEE Trans. Energy Convers. 20 (2) (2005) 268–275, http://dx.doi.org/10.1109/TEC.2005.847970.

[34] T. Szolc, R. Konowrocki, M. Michajlow, A. Pregowska, An investigation of the dynamic electromechanical coupling effects in machine drive systems driven by asynchronous motors, Mech. Syst. Signal Process. 49 (1–2) (2014) 118–134, http://dx.doi.org/10.1016/j.ymssp.2014.04.004.

[35] G. Slemon, Modelling of induction machines for electric drives, IEEE Trans. Ind. Appl. 25 (6) (1989) 1126–1131, http://dx.doi.org/10.1109/28.44251.

[36] M. Hinkkanen, A.-K. Repo, M. Cederholm, J. Luomi, Small-signal model for saturated deep-bar induction machines, in: 2007 European Conference on Power Electronics and Applications, IEEE, Aalborg, Denmark, 2007, pp. 1–10, http://dx.doi.org/10.1109/EPE.2007.4417769.

[37] A. Repo, A. Arkkio, Numerical impulse response test to estimate circuit-model parameters for induction machines, IEE Proc. - Electr. Power Appl. 153 (6) (2006) 883, http://dx.doi.org/10.1049/ip-epa:20060047.

[38] A.-K. Repo, P. Rasilo, A. Niemenmaa, A. Arkkio, Identification of electromagnetic torque model for induction machines with numerical magnetic field solution, IEEE Trans. Magn. 44 (6) (2008) 1586–1589, http://dx.doi.org/10.1109/TMAG.2007.916143.

[39] L. Tiitinen, M. Hinkkanen, L. Harnefors, Design framework for sensorless control of synchronous machine drives, IEEE Trans. Ind. Electron. (2024) 1–12, http://dx.doi.org/10.1109/TIE.2024.3429650.

[40] M. Hinkkanen, A.-K. Repo, M. Cederholm, J. Luomi, Small-signal modelling of saturated induction machines with closed or skewed rotor slots, in: Industry Applications Annual Meeting, IEEE, 2007, p. 7.

[41] T. Holopainen, A.-K. Repo, J. Järvinen, Electromechanical interaction in torsional vibrations of drive train systems including an electrical machine, in: Proceedings of the 8th IFToMM International Conference on Rotordynamics, Seoul, South Korea, 2010.

[42] H. Hartikainen, L. Tiitinen, S. Laine, M. Hinkkanen, Identification of mechanical impedance of an electric machine drive for drivetrain design, in: 2023 IEEE International Electric Machines & Drives Conference, IEMDC, 2023, pp. 1–6, http://dx.doi.org/10.1109/IEMDC55163.2023.10238992.

[43] L. Tiitinen, H. Hartikainen, L. Peretti, M. Hinkkanen, motulator: Motor drive simulator in Python, in: 2023 IEEE International Electric Machines & Drives Conference, IEMDC, 2023, pp. 1–7, http://dx.doi.org/10.1109/IEMDC55163.2023.10238938.